Microwave Land Emissivity Calculations Using AMSU Measurements

Fatima Karbou, Catherine Prigent, Laurence Eymard, and Juan R. Pardo

***Abstract*—Atmospheric parameter retrievals over land from Advanced Microwave Sounding Unit (AMSU) measurements, such as atmospheric temperature and moisture profiles, could be possible using a reliable estimate of the land emissivity. The land surface emissivities have been calculated using six months of data, for 30 beam positions (observation zenith angles from $-58°$ to $+58°$) and the 23.8-, 31.4-, 50.3-, 89-, and 150-GHz channels. The emissivity calculation covers a large area including Africa, Eurasia, and Eastern South America. The day-to-day variability of the emissivity is less than 2% in these channels. The angular and spectral dependence of the emissivity is studied. The obtained AMSU emissivities are in good agreement with the previously derived SSMI ones. The scan asymmetry problem has been evidenced for AMSU-A channels. And possible extrapolation of the emissivity from window channels to sounding ones has been successfully tested.**

***Index Terms*—Advanced Microwave Sounding Unit (AMSU), microwave surface emissivity.**

I. Introduction

PASSIVE microwave measurements from the Advanced Microwave Sounding Unit (AMSU) A and B onboard the National Oceanic and Atmospheric Administration (NOAA) polar orbiting satellites are increasingly used over ocean in operational numerical weather prediction (NWP) models.

The AMSU-A sounding channels are used for atmospheric temperature profile retrievals whereas the AMSU-B channels are designed for atmospheric humidity profiling. In addition, AMSU window channels are sensitive to the surface, cloud, and rain, and can be used to derive many parameters such as total precipitable water, sea ice concentration, precipitation rate, or cloud liquid water (e.g., see [8], [28], and [31]). However, AMSU profiling information is still insufficiently exploited over land. The land surface emissivity is high (often close to 1.0) as compared to the ocean one and experiences strong temporal and spatial variations with surface types, roughness, and moisture content, among other parameters. Consequently, it is more difficult to discriminate between the surface and atmosphere contributions over land than over ocean. So far, only the profiling channels that are not sensitive to the surface are operationally used over land. English [4] showed that the use of land emissivity with accuracy better than 2% would help humidity profile retrievals over land. The present study is essentially motivated by the need to improve the low-level atmospheric temperature and humidity profiles retrievals over land. It is crucial to estimate accurate land surface emissivities at a global scale for the AMSU channels in order to allow accurate retrievals of the temperature and humidity in the lower atmospheric layers.

Various emissivity model developments have been conducted (e.g., see [12] and [29]), but the modeling approaches for global applications are hampered by: 1) the complexity of the interaction between the radiation and the large variability of the medium encountered over the globe and 2) the lack of accurate input parameters to feed the model (vegetation characteristics, soil moisture, roughness, among others). Ground-based and aircraft measurements of land surface emissivities have been performed, but their extrapolation to surfaces at larger scales is questionable. Airborne microwave measurements have been used to estimate land surface emissivity of forest and agricultural areas [9], and snow and ice surfaces [10] at 24, 50, 89, and 150 GHz. Moreover, ground-based microwave emissivity measurements have been performed over variety of vegetation types from bar soils to vegetated areas (see [1], [15], [16], and [30], among others).

Land emissivity studies at regional to global scales have already been carried out directly from satellite measurements. Prigent *et al.* [23], [24] estimated the microwave land emissivities over the globe at the frequencies of the Special Sensor Microwave/Imager (SSMI) channels (19, 22, 35, and 85 GHz) for vertical and horizontal polarizations, at 53° zenith angle by removing the atmosphere, clouds, and rain contributions using ancillary satellite data. Extrapolation of these estimates to AMSU-A frequencies and scanning conditions has been attempted [22]. Other emissivity calculations have been performed for limited geographic areas. Felde and Pickle [5] retrieved surface emissivities at 91 and 150 GHz for cloud-free data from SSM/T2 atmospheric water vapor profiler and radiosonde measurements. Choudhury [2] calculated the surface reflectivity at 19 and 37 GHz using SSMI/I data over different surface types. Jones and Vonder Haar [13] proposed a method to routinely generate the microwave land emissivity, using

Manuscript received May 18, 2004, 2004; revised September 29, 2004. The work of J. Pardo was supported by the Spanish DGES and PNIE under Grants ESP2002-01627, AYA2002-10113-E, and AYA2003-02785-E.

F. Karbou was with the Centre National de la Recherche Scientifique (CNRS), Centre d' étude des Environnements Terrestre et Planétaires (CETP), 78140 Vélizy, France. She is now with the CNRS, Centre National de Recherches Météorologiques (CNRM), Météo-France, 31057, Toulouse Cedex 1, France (e-mail: fatima.karbou@cnrm.meteo.fr).

C. Prigent is with the Centre National de la Recherche Scientifique (CNRS), Observatoire de Paris, 75014, Paris, France.

L. Eymard is with the Centre National de la Recherche Scientifique (CNRS), Laboratoire d'Océanographie Dynamique et de Climatologie (LODYC), 75252, Paris, France.

J. R. Pardo is with Consejo Superior de Investigaciones Cientificas, IEM-DAMIR, Serrano 121, 28006, Madrid, Spain.

Digital Object Identifier 10.1109/TGRS.2004.837503

microwave and infrared satellite data. Morland *et al.* [18] used SSM/I data to compute surface emissivities in semiarid areas. Similar surface types have been previously sensed using microwave aircraft observations to derive land surface emissivity from 24–157 GHz [19].

The goal of this study is to calculate reference land surface emissivity maps at AMSU frequencies and scanning conditions, directly using AMSU observations. The procedures are to get the land emissivities at 23.8, 31.4, 50.3, 89, and 150 GHz for all AMSU zenith angles by removing the contribution of the atmosphere, clouds, and rain. The International Satellite Cloud Climatology Project (ISCCP) data is used to identify cloud-free AMSU observations and to provide an accurate value of the skin temperature [27]. The European Centre for Medium-Range Weather Forecasts (ECMWF) temperature-humidity profiles are used to input the Atmospheric Transmission at Microwave (ATM) radiative transfer model that calculates the cloud-free atmospheric contribution [20]. Results are presented for six months of AMSU data in 2000, covering a large geographic area (from $-60°$ to $+60°$ in longitudes and latitudes). The emissivity retrieval scheme (data and method) for AMSU window channels is described in Section II and an error analysis is conducted. The angular and spectral variations of the AMSU emissivities are characterized (Section III), and the day-to-day variability is briefly discussed. Extrapolation to the AMSU sounding channels is tested in Section IV. Section V provides the conclusions.

TABLE I
AMSU-A/B CHANNEL CHARACTERISTICS

Channel No	Frequency (GHz)	Sensitivity (K)	Resolution at nadir (km)
	AMSU-A		
1	23.8	0.20	48
2	31.4	0.27	48
3	50.3	0.22	48
4	52.8	0.15	48
5	53.596+/-0.115	0.15	48
6	54.4	0.13	48
7	54.9	0.14	48
8	55.5	0.14	48
9	57.290=f_0	0.20	48
10	f_0 +/- 0.217	0.22	48
11	f_0 +/- 0.322 +/- 0.048	0.24	48
12	f_0 +/- 0.322 +/- 0.022	0.35	48
13	f_0 +/- 0.322 +/- 0.010	0.47	48
14	f_0 +/- 0.322 +/- 0.0045	0.78	48
15		0.11	48
	AMSU-B		
16	89	0.37	16
17	150	0.84	16
18	183.31 +/- 1	1.06	16
19	183.31 +/- 3	0.70	16
20	183.31 +/- 7	0.60	16

II. LAND SURFACE EMISSIVITY CALCULATION FOR AMSU WINDOW CHANNELS

A. Data

The AMSU sounding unit is operational onboard the NOAA 15 satellite since 1998. It contains two modules A and B. The first one, AMSU-A measures the outgoing radiation from the earth's surface and from different atmospheric layers using 15 spectral regions (23.8–89.0 GHz). The sounding channels (52.8–58 GHz) are used to retrieve the atmospheric temperature information from about 3 hPa (45 km) to the earth's surface. AMSU-A is composed of two separate units: AMSU-A1 with 12 channels in the frequency range 50–60-GHz bands and one channel at 89 GHz, and AMSU-A2 unit with 2 surface channels at 23.8 and 31.4 GHz. Moreover, the AMSU-A1 unit benefits of two antenna systems to provide measurements from 50–89 GHz. AMSU-B is designed for humidity sounding and has two window channels at 89 and 150 GHz and three other channels centered on the 183.31-GHz water vapor line. AMSU A and B have a nominal field of view of 3.3° and 1.1° and sample 30 and 90 earth views, respectively. Thereby, the AMSU observation scan angle θ_s varies from $-48°$ to $+48°$. Consequently, the corresponding local zenith angle could reach 58°. Channel characteristics for both AMSU-A and AMSU-B radiometers are given in Table I and a detailed description of the AMSU sounders is reported in [7]. In the present study, level 1b AMSU data from year 2000 have been obtained from the Satellite Active Archive (SAA) and processed using the Advanced ATOVS Processing Package (AAPP) created and distributed by European Organization for the Exploitation of Meteorological Satellites (EUMETSAT) and other partners. The AMSU radiances are corrected from the AMSU antenna effect [11], [17].

Clouds have a complex impact on the observed microwave radiances. Therefore, cloudy situations should not be accounted for in the emissivity calculation. Cloud parameters and skin temperature are extracted from the ISCCP pixel level data (the DX dataset) for year 2000. These parameters are available at 30-km ground resolution and every 3 h. Within ISCCP, information about clouds is obtained from visible and infrared measurements from polar and geostationary satellites, using radiative analysis [27]. With an infrared emissivity close to 1.0, observations in the thermal infrared region can provide estimates of the surface skin temperature in cloud-free situations. In the assumption of unit surface emissivity, clear infrared radiances are used by the ISCCP processing to derive estimates of the skin temperature. The retrieved skin temperatures are further corrected to account for the emissivity change with surface types. The skin temperature accuracy is assumed to be within 4 K as reported by Rossow and Garder [25], [26].

The cloud-free atmospheric contribution is calculated via radiative transfer simulations using as input the ECMWF temperature-humidity profiles. The profiles we used are from the ECMWF ERA40 reanalysis for 2000 available globally, every 6 h, for 60 vertical pressure levels, and for a horizontal grid resolution of $1.125° \times 1.125°$.

TABLE II
AMSU EMISSIVITY SENSITIVITY TO ERRORS IN THE (a) AIR HUMIDITY PROFILES, (b) AIR TEMPERATURE PROFILES, (c) SKIN TEMPERATURE, AND (d) INSTRUMENT BRIGHTNESS TEMPERATURE

Frequencies (GHz)	$\theta <= 45°$ 30200 points	$\theta > 45°$ 6886 points	TPW <= 30 g/m^2 26472 points	TPW > 30 g/m^2 10616 points
	Air humidity errors (mean/std)			
23.8	-0.001 / 0.001	-0.002 / 0.002	-0.001 / 0.001	-0.001 / 0.003
31.4	-0.001 / 0.001	-0.002 / 0.002	-0.001 / 0.001	-0.003 / 0.003
50.3	-0.001 / 0.001	-0.002 / 0.002	-0.001 / 0.001	-0.003 / 0.004
89.0	-0.005 / 0.005	-0.009 / 0.008	-0.006 / 0.004	-0.010 / 0.014
150	-0.004 / 0.015	-0.006 / 0.035	-0.007 / 0.012	0.023 / 0.056
	Air temperature errors (mean/std)			
23.8	-0.001 / 0.001	-0.001 / 0.001	-0.001 / 0.001	-0.002 / 0.001
31.4	-0.001 / 0.001	-0.001 / 0.001	-0.001 / 0.001	-0.001 / 0.001
50.3	-0.005 / 0.001	-0.010 / 0.001	-0.006 / 0.002	-0.008 / 0.003
89.0	-0.002 / 0.001	-0.003 / 0.003	-0.002 / 0.001	-0.008 / 0.004
150	-0.008 / 0.010	-0.017 / 0.027	-0.007 / 0.007	-0.045 / 0.036
	Skin temperature errors (mean/std)			
23.8	-0.028 / 0.002	-0.029 / 0.002	-0.028 / 0.002	-0.031 / 0.002
31.4	-0.028 / 0.002	-0.027 / 0.002	-0.027 / 0.002	-0.028 / 0.002
50.3	-0.036 / 0.003	-0.041 / 0.004	-0.037 / 0.003	-0.038 / 0.004
89.0	-0.030 / 0.002	-0.031 / 0.004	-0.030 / 0.002	-0.035 / 0.004
150	-0.037 / 0.009	-0.042 / 0.016	-0.037 / 0.008	-0.062 / 0.017
	Instrument brightness temperature errors (mean/std)			
23.8	0.008 / 0.001	0.009 / 0.001	0.008 / 0.001	0.011 / 0.001
31.4	0.008 / 0.001	0.008 / 0.001	0.008 / 0.001	0.008 / 0.001
50.3	0.015 / 0.002	0.021 / 0.003	0.016 / 0.003	0.018 / 0.004
89.0	0.010 / 0.002	0.012 / 0.004	0.010 / 0.002	0.017 / 0.005
150	0.024 / 0.027	0.054 / 0.102	0.021 / 0.017	0.138 / 0.151

B. Emissivity Calculation

In the AMSU microwave frequencies range, for a non scattering plane-parallel atmosphere and, for a given path zenith angle, the brightness temperature (Tb) observed by the satellite instrument can be expressed as

$$Tb_{(p,\vartheta)} = \left(T_{skin} \times \varepsilon_{(p,\vartheta)} \times \Gamma\right) + \left(T_{(\vartheta,\downarrow)} \times \left(1 - \varepsilon_{(p,\vartheta)}\right) \times \Gamma\right)\Big] + T_{(\vartheta,\uparrow)} \quad (1)$$

$$\Gamma = \exp\left(\frac{-\tau_{(0,H)}}{\cos(\theta_z)}\right). \quad (2)$$

$T_{b(p,\upsilon)}$ and $\varepsilon_{(p,\upsilon)}$ are the instrument Tb and the surface emissivity at frequency υ and for polarization p, respectively. T_{skin}, $T_{(\upsilon,\downarrow)}$ and $T_{(\upsilon,\uparrow)}$ are the skin temperature, the upwelling and the downwelling Tbs respectively. Γ is the net atmospheric transmissivity.

Equation (1) leads to the land emissivity expression

$$\varepsilon_{(p,\vartheta)} = \frac{\left(Tb_{(p,\vartheta)} - T_{(\vartheta,\uparrow)} - T_{(\vartheta,\downarrow)} \times \Gamma\right)\Big]}{\left(\left(T_{skin} - T_{(\vartheta,\downarrow)}\right) \times \Gamma\right)}. \quad (3)$$

For the emissivity estimation, we took into account all AMSU cloud-free observations and all AMSU-A zenith angles (30 values from $-58°$ to $+58°$). The radiative transfer computations are performed using the ATM model. This model, based on different developments and measurements described in [20], is fully applicable in the 0–1600-GHz frequency range and has been evaluated by intercomparisons with other existing radiative transfer models [6].

C. Emissivity Sensitivity to Errors in the Input Parameters

So far, there are no extensive in-situ emissivity measurements that could be compared to the retrieved emissivity in order to directly evaluate the emissivity estimate errors. Therefore, the accuracy of the estimated microwave emissivity to errors in the input parameters is evaluated by analyzing its change due to a variation in one of them, the other parameters remaining unchanged. The accuracy evaluation is performed for five days of AMSU-A and B cloud-free data from early January 2000.

For example, the impact of humidity profile errors on the microwave emissivity is estimated by calculating the emissivity variation due to an alteration of $\pm 15\%$ in the humidity profile. The same approach is used to determine the emissivity variation due to the air temperature profile (± 1 K at all pressure levels), to the instrument Tb (± 1 K), and to the skin temperature (± 4 K). The emissivity variations are calculated at 23.8, 31.4, 50.3, 89, and 150 GHz, for four observation classes 1) low zenith angles ($< 45°$); 2) high zenith angles ($> 45°$); 3) dry atmospheres (Total Water Vapor Content (TWVC) < 30 kg/m^2); and 4) moist conditions (TWVC > 30 kg/m^2). The corresponding results are given in Table II. Calculations are not shown for the other AMSU frequencies that are located near the oxygen and water vapor lines. At these frequencies with low atmospheric transmission, the surface contribution to the measured radiation is not large enough to provide reliable emissivity estimates. In the following section, the emissivity frequency dependence will be discussed and a solution will be provided and tested to estimate the emissivities in these opaque channels from the near-by window frequency observations.

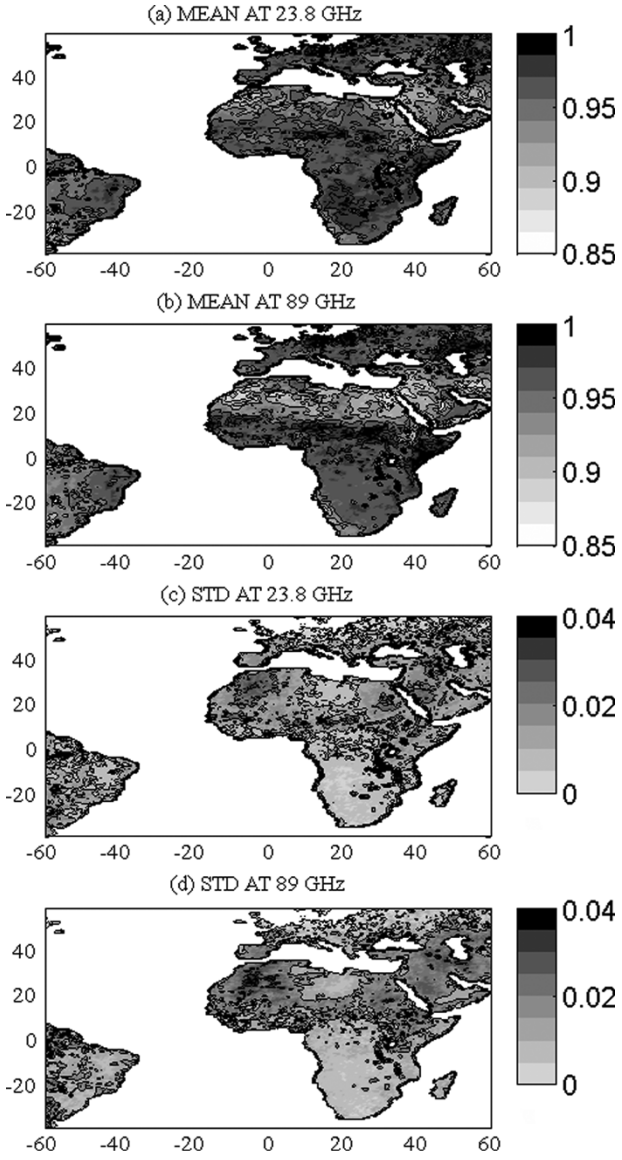

Fig. 1. (a) Mean emissivity for July 2000 for low zenith angles ($\leq 45°$) at 23.8 GHz, (b) same as (a) but at 89 GHz, (c) emissivity standard deviation for July 2000 for low zenith angles (($\leq 45°$) at 23.8 GHz, (d) same as (c) but at 89 GHz.

Table II shows that for all window channels, the emissivity decreases when the air mixing ratio, the surface temperature, or air temperature increases. On the contrary, an increase in the instrument Tb enhances the estimated emissivity. At all frequencies, the emissivity variation due to errors in one input parameter is larger for high TWVC and for high observation zenith angles this is explained by the fact that increasing TWVC as well as increasing zenith angle result on a decrease in the atmospheric transmissivity and, therefore, less sensitivity to the surface contribution. Errors in the humidity profiles have little effects on the surface channels 23.8, 31.4, and 50.3 GHz (less than 0.25% of relative error $(d\varepsilon/\varepsilon)$).

However, their impact is greater on the 89- and 150-GHz emissivities in dry atmospheres or for low zenith angles, the emissivity sensitivity is five times greater at these two channels than at the 23.8-GHz one. This effect is enhanced for very moist conditions and large zenith angles, with errors rising up to 1.1% at 89 GHz and 4% at 150 GHz. Errors in skin temperatures greatly influence the retrieved emissivity at all frequencies. For dry conditions, the emissivity relative errors are about 3% for 23.8 and 31.4 GHz, 3.5% at 50 and 89 GHz, and 4% at 150 GHz. As expected, errors in the air temperature profile produce larger emissivity variations at 50 GHz than at other frequencies that are located farther away from the oxygen absorption bands.

In order to reduce the calculation errors, the emissivity calculations will be averaged over a certain period of time. The time variability will be analyzed and compared to the theoretical noise errors previously calculated. Note that contrarily to SSM/I observations, AMSU measurements are performed at various incidence angles, thus limiting the number of overpasses per location with the same observation conditions.

TABLE III
BIOSPHERE–ATMOSPHERE TRANSFER SCHEME (BATS) VEGETATION CLASSES

Classes	Legend	Total number of selected AMSU observations during January 2000
1	Crops, Mixed Farming	28819
2	Short Grass	15570
3	Evergreen Needleleaf Trees	1459
4	Deciduous Needleleaf Tree	218
5	Deciduous Broadleaf Trees	4419
6	Evergreen Broadleaf Trees	11253
7	Tall Grass	22444
8	Desert	90797
9	Tundra	123
10	Irrigated Crops	167
11	Semi-desert	28876
12	Ice Caps and Glaciers	0
13	Bogs and Marshes	850
14	Inland Water	0
16	Evergreen Shrubs	2134
17	Deciduous Shrubs	3994
18	Mixed Forest	1263
19	Interrupted Forest	43166
20	Water and Land Mixtures	0

III. AMSU LAND EMISSIVITY ANALYSIS

A. Emissivity Maps

Monthly mean emissivity maps are shown in Fig. 1(a) and 1(b), at 23.8 and 89 GHz, respectively, for July 2000, averaged over zenith angles lower than 45°. All available cloud-free AMSU observations are used to produce these maps at a 30 × 30 km resolution. The corresponding emissivity standard deviation maps are also presented [Fig. 1(c) and 1(d)].

The monthly mean emissivity maps show expected spatial structures, related to changes in surface types. Lakes and rivers as well as the coastlines are associated with low emissivities at all frequencies. Compared to other medium, water has high dielectric values that translate into low emissivities. The Victoria, Malawi, and Tanganyika lakes are easily distinguished.

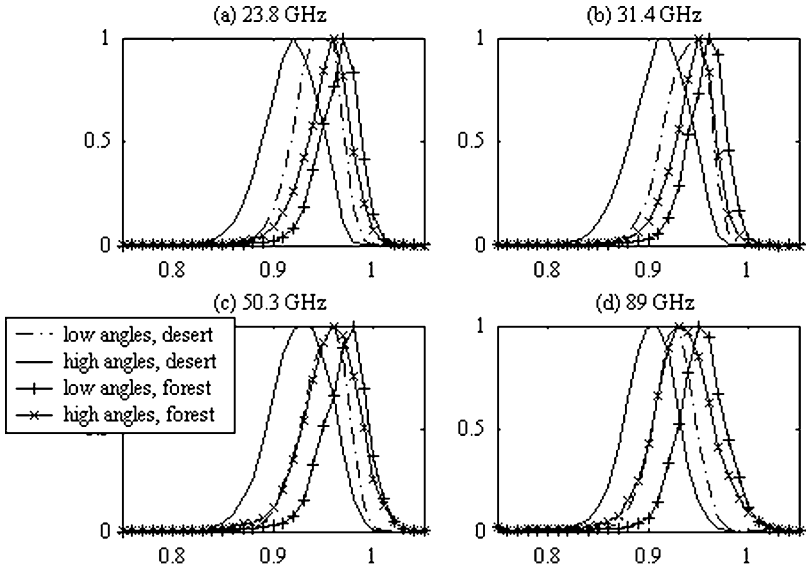

Fig. 2. Histograms of the emissivity from February 2000, for low zenith angles and desert (angles $\leq 45°$, dashed-dotted curve), for high zenith angles and desert (angles $> 45°$, solid curve), for low zenith angles and forest (solid curve with plus symbols) and for high zenith angles and forest (solid curve with cross symbols) at (a) 23.8 GHz, (b) 31.4 GHz, (c) 50.3 GHz, and (d) 89 GHz.

Open water areas are also associated with the highest emissivity variability [see Fig. 1(c) and (1d)]. At the border between land and open water, the percentage of each contribution (land and water) can change between two satellite overpassings because they are not perfectly coincident in space, leading to significant emissivity changes. The emissivity also changes with vegetation cover. We used the Biosphere–Atmosphere Transfer Scheme (BATS) dataset (available at 30 $\times$ 30 km grid resolution) for land cover classification [3]. Table III lists the different land cover classes available in the dataset. Bare soil areas (like desert regions in North Africa and Arabia) are characterized by lower emissivity. They have a quasi-specular behavior. On the other hand, dense vegetation areas have a quasi-Lambertian reflection associated to rather high emissivity. This is confirmed by the emissivity histograms calculated using February 2000 data at 23.8, 31.4, 50.3, and 89 GHz [Fig. 2(a)–(d), respectively]. The histograms are established for two zenith angle classes (angles $<= 45°$ and angles $> 45°$) and for desert and dense vegetation areas [see Fig. 2(a)–(d)]. As expected, and for all frequencies, the emissivity is higher at low zenith angles than at higher ones for desert areas. The emissivity change due to the zenith angle (difference between the mean emissivity for low angles and the mean emissivity for high angles) is about 0.024 for 23.8 and 31.4 GHz and 0.023 for 50.3 and 89 GHz. The emissivity change for a dense vegetation area is smaller: less than 0.009 for channels 1 and 2 and about 0.01 for the two others. We examine in detail the emissivity variation depending on zenith angle in the next section. In the desert, two particular areas of very low emissivities will be noted, one in the south of Arabia (Western Oman, Eastern Yemen) and another one in Egypt. These regions also show low emissivities on the maps derived from SSM/I observations. They have been showed to be related to geological structures [21] but no final explanation exists yet despite on-going assiduous investigations (dielectric measurement of rocks and sand from those regions along with modeling studies).

B. Day-to-Day Emissivity Variations

As shown by Fig. 1(c) and (d), the day-to-day emissivity standard deviations for 1 month are generally within 0.02 for all channels, i.e., within the required theoretical limit calculated by English [4]. As expected, they tend to increase with frequency, given the increasing sensitivity to atmospheric contamination and sensitivity to surface errors (see Section II-C). As already discussed, areas with higher variations are often associated with the presence of standing water (coastal areas, flood regions). For the month of July shown here (Fig. 1), the subsahelian transition zone in Africa is associated with rather large emissivity variations. This fact is likely related to the rainy season in this region at this period of the year with two consequences 1) potential cloud contamination is likely; 2) rain-induced soil moisture variation along with the corresponding vegetation changes can lead to important emissivity variations.

In order to further evaluate the day-to-day variation of the estimated emissivity, two areas with different vegetation cover have been selected. We calculate for them the mean daily emissivity during the month of January 2000 at 23.8, 31.4, 50.3, 89, and 150 GHz. To avoid the emissivity variation due to the zenith angles, data at angles less than 45° are selected. Moreover, all water pixels (lakes and rivers) are removed for the calculation to avoid the emissivity change between land and water surfaces.

The calculation results are shown on Fig. 3(a)–(f). Fig. 3(a), (c), and (e) shows the day-to-day variation of the emissivity over a desert area in Mauritania (15W 10W; 20N 25N) at 23.8, 89, and 150 GHz, respectively. The mean emissivity curve has the same trend for all frequencies. Error bars are larger for 89 and 150 GHz, which is consistent with the error analysis provided in the Section II-C. The emissivity variation is not only due to errors in the input parameters: it can also correspond to real changes in surface properties. Between day 15 and day 20, a significant emissivity decrease can be observed. We checked on the ISCCP cloud dataset that it corresponds to the overpassing of

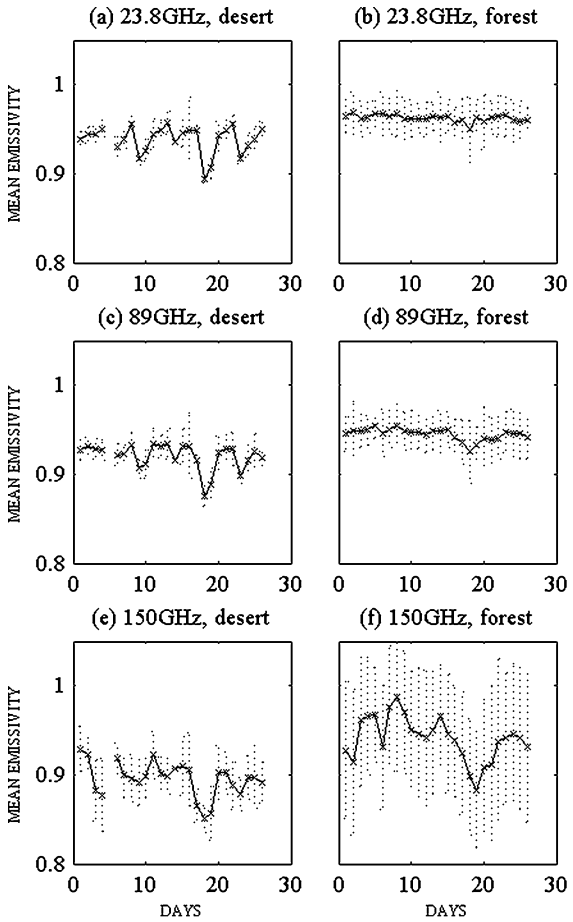

Fig. 3. Day-to-day variation of the emissivity over a desert surface at (a) 23.8, (c) 89, and (e) 150 GHz and over a tropical forest in Africa at (b) 23.8, (d) 89, and (f) 150 GHz.

a significant convective activity in the region, likely associated to rain and induced soil moisture increase. Fig. 3(b), (d), and (f) presents the day-to-day variation of the emissivity over a tropical forest in Africa (18W 10W; 0N 10N) at 23.8, 89, and 150 GHz, respectively. For all channels (except the 150 GHz), the emissivity remains almost unchanged during the month. At 150 GHz, the emissivity is associated with large daily variability that can be related to the sensitivity of this channel to input errors especially for high TWVC situations.

C. Angular Dependence of the AMSU Emissivity

The cross-track scanning pattern of the AMSU instrument provides observation angles between $\pm 58^\circ$. In addition, because of the rotating AMSU antenna, the estimated emissivity is a mixture between the vertical and the horizontal polarizations. The AMSU emissivity at scan angle θ_z could be written as follows:

$$\varepsilon(\theta_z) = \varepsilon_p(\theta_z) \times \cos^2(\theta_s) + \varepsilon_q(\theta_z) \times \sin^2(\theta_s) \qquad (4)$$

where $\varepsilon_p(\theta_z)$ and $\varepsilon_q(\theta_z)$ are the two orthogonal polarized surface emissivities at θ_z local zenith angle. For AMSU surface channels, the polarization is vertical near nadir and thereby, ε_p is equal to ε_v and ε_q is equal to ε_h.

In order to examine the emissivity variation with the zenith angle, the calculated emissivities have been sorted by beam position and vegetation type (nadir corresponds to scan positions 15 and 16). The resulting monthly mean emissivities for desert and dense vegetation are presented on Fig. 4 for January and August 2000. Regarding each vegetation class, SSMI emissivities for January 1993 and August 1992 (obtained from Prigent *et al.* [24]) at 19, 37, and 85 GHz and for 53° zenith angle (scan positions 2 and 29), recalculated for an AMSU like polarization [using (4)] are added to the plots for comparison. For example, at 23.8 GHz, we add the estimated SSMI emissivity at 19 GHz for 53°. For both vegetation types and for all channels, we notice a very good agreement between the AMSU emissivities at zenith angles close to 53° and the SSMI ones. The figure shows the strong dependence of the AMSU emissivity with the zenith angles over desert areas. We observe the same behavior over semi-desert areas (see Fig. 5). For forested areas, the dependence is much smaller, as expected: dense vegetation is associated with quasi-Lambertian reflection and thereby the observation angle has a limited impact. Additional plots using January data are provided on Fig. 5, for nine vegetation classes and for all surface channels (23–150 GHz).

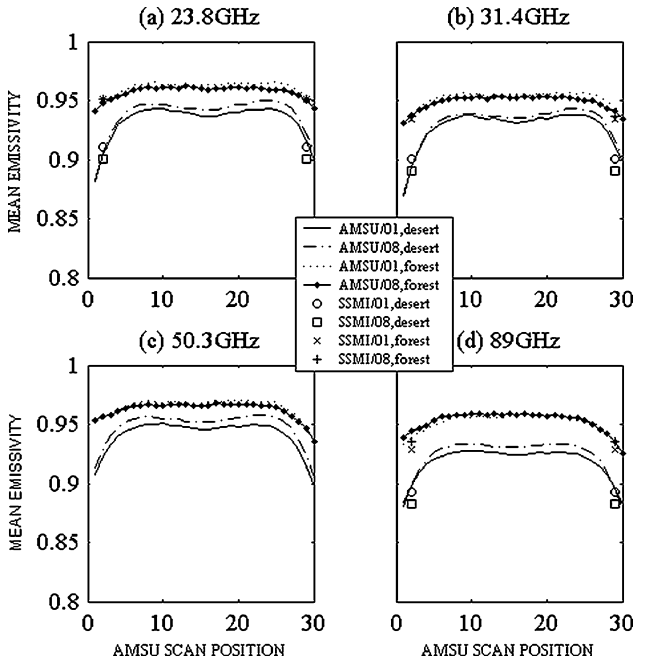

Fig. 4. Monthly mean AMSU emissivities with respect to 30 scan positions ($\pm 58^\circ$ of zenith angle variation) and two surface types desert (solid lines for January and dashed–dotted lines for August) and forest (dotted lines for January and solid-dotted lines for August). (a) At 23.8 GHz with SSMI emissivities at 53° and at 19 GHz, (b) same as (a) but at 31.4 GHz with SSMI emissivities at 37 GHz, (c) same as (a) but at 50.3 GHz, and (d) same as (a) but at 89 GHz with SSMI emissivities at 85 GHz.

The results show also an asymmetry along the AMSU scan, relatively to nadir, variable with frequency and surface emissivity. To highlight this effect, we have calculated the difference between the monthly mean emissivities at the scan edges (scan positions 1 and 30) for different vegetation covers, for six months of data, at 23.8, 31.4, 50.3, and 89 GHz (see Fig. 6). For all surfaces, the asymmetry (monthly mean emissivity at scan position 30 minus the monthly mean emissivity at scan position 1) is always positive for 23.8 and 31.4 GHz (both channels are located on the AMSU-A1 module) and always negative for 50.3 and 89 GHz (measurements at these frequencies

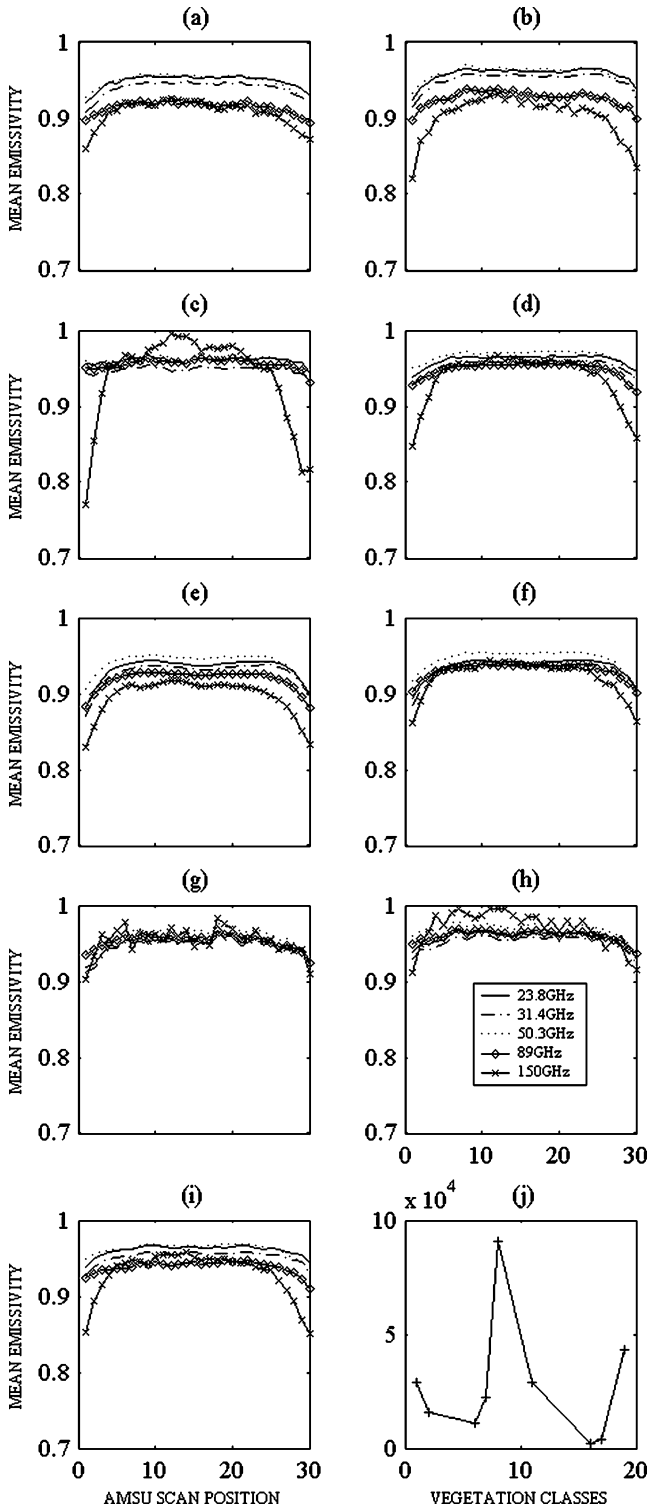

Fig. 5. Monthly mean AMSU emissivities for January 2000 with respect to 30 scan positions ($\pm 58^\circ$ of zenith angle variation) and nine surface types at 23.8, 31.4, 50.3, 89, and 150 GHz. The sample size curve for each vegetation class (see Table II) is plotted on (j). (a) Crops, mixed farming, (b) short grass, (c) evergreen broadleaf trees, (d) tall grass, (e) desert, (f) semi-desert, (g) evergreen shrubs, (h) deciduous shrubs, (i) interrupted forest, and (j) sample size.

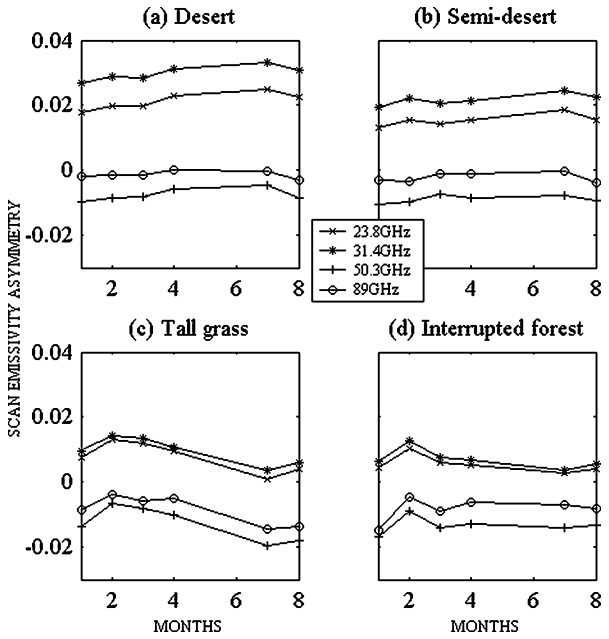

Fig. 6. Monthly scan asymmetry (monthly mean emissivity at scan position 30, minus monthly mean emissivity at scan position 1) for 23.8 GHz (solid lines with cross symbol), 31.4 GHz (solid lines with star symbol), 50 GHz (solid lines with plus symbol), and 89 GHz (solid lines with circle symbol) regarding. (a) Desert, (b) semi-desert), (c) tall grass, and (d) interrupted forest.

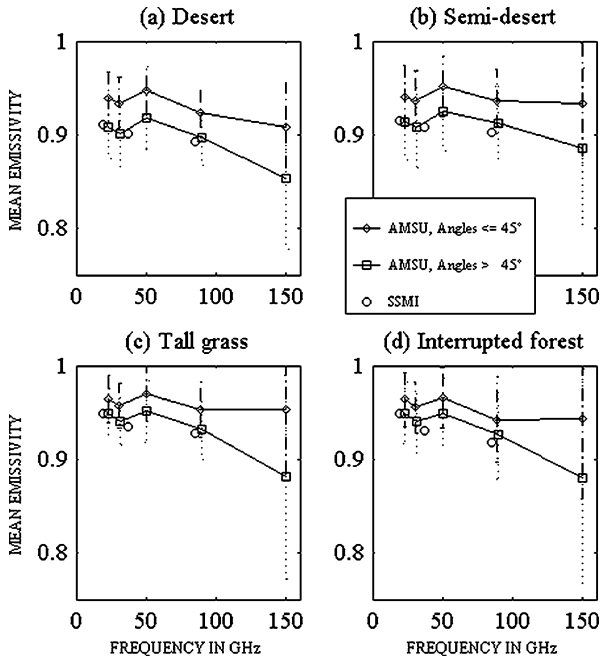

Fig. 7. Monthly mean emissivities from January 2000 with respect to the frequency for low zenith angles ($\leq 45^\circ$, solid lines with diamond symbols) and high zenith angles ($> 45^\circ$, solid lines with square symbol) for (a) desert, (b) semi-desert, (c) tall grass, and (d) interrupted forest. For each vegetation class, the corresponding SSMI emissivities at 19, 37, and 85 GHz (circle symbols) are added as well as the AMSU emissivity standard deviations.

are obtained from the AMSU-A2 module). For all vegetation classes, the AMSU scan asymmetry is higher at 31.4 GHz than at the other frequencies. The maximum bias at this frequency is about 0.033 and is observed over desert surfaces (surface with the lowest emissivity). Notice that 0.033 in emissivity scan asymmetry could represent 9 K in terms of Tb (assuming a skin temperature of 300 K and an atmospheric transmissivity of 0.9). Channel 2 (23.8 GHz) is located on the same module (AMSU-A1) than channel 1 (31.4 GHz), but is less sensitive to the asymmetry; the maximum asymmetry is less than 0.024. Measurements at 89 GHz appear to be less sensitive to the scan

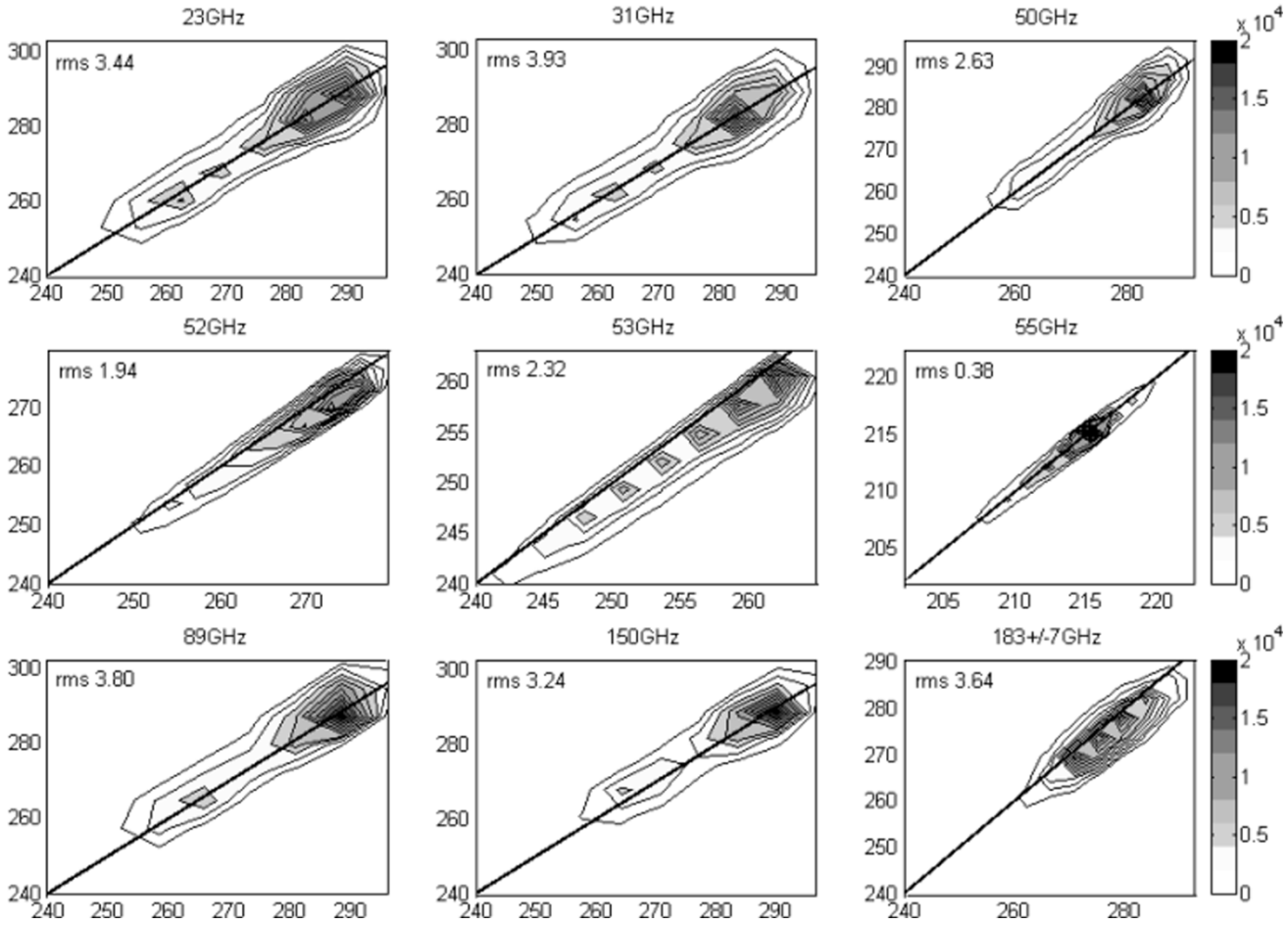

Fig. 8. Density contours of the observed brightness temperature (X axis) versus the simulated brightness temperature (Y axis) over land using odd January 2000 days data for AMSU channels 23.8, 31.4, 50.3, 52.8, 53, 89, 150, and 183 $+/-$ 7 GHz. The RMS of errors for (observations-simulations) is added to the plots. The color bar indicates the observations number for each contour class.

asymmetry than those at 50.3 GHz. Weng *et al.* [28] also noticed an asymmetry in the AMSU 31-GHz channel by using observations and simulations over an ocean background surface. The AMSU scan asymmetry could be related to an instrument problem. For performant retrievals of atmospheric parameter over ocean and land, the instruments have to be accurately calibrated for all conditions (frequencies and scanning positions). Further studies should investigate this asymmetry problem over land and ocean surfaces to suggest adequate corrections.

D. Frequency Dependence of the AMSU Emissivity

Fig. 7 shows the monthly mean emissivities for dry and vegetated surfaces calculated using January data, at AMSU window channels between 23.8 and 150 GHz and for high ($> 45°$) and low ($\leq 45°$) zenith angles. For comparison purposes, SSMI emissivities at 19, 3, 7, and 85 GHz, at 53° for January 1993 are added to the plots [using the polarization mixing from (4)]. For bare soil [Fig. 7(a) and (b)] and vegetated areas [Fig. 7(c) and 7d)], the frequency dependence of the AMSU emissivities at high zenith angles is in very good agreement with the ones derived from SSM/I estimates. For all considered vegetation classes and both high and low zenith angles, the emissivity slightly decreases from 23–31 GHz and then increases at 50 GHz.

The amplitude of the increase at 50 GHz does not depend significantly upon scan angle or TWVC (similar trend over desert and tropical forest). This could be due at least to two factors: absolute instrument calibration error at 50 GHz and systematic errors in the gaseous absorption calculation at this frequency. Additional investigations have to be performed, both over ocean and land to understand this problem. At 23.8, 31.4, and 50 GHz, error bars have the same magnitude for low zenith angles and for all surface types and are smaller than at 89 and 150 GHz. For all channels, the error bars increase with increasing zenith angles. The channels 89 and 150 GHz are more sensitive to residual atmospheric errors leading to increasing error bars; this effect is intensified at 150 GHz for moist conditions and high zenith angles. The observed emissivity decreases in vegetated areas at high zenith angles between 89 and 150 GHz is not realistic. In Section II-C, it has been shown that the 150-GHz channel is particularly sensitive to errors in all calculation input parameters. This is also evidenced by the large error bars associated with the emissivity estimates at this frequency (almost 0.07 for tall grass vegetation type as compared to 0.03 for the other frequencies). For low zenith angles, the emissivity does not change much from 89 and 150 GHz for both dry and vegetated areas: the emissivity estimate at 150 GHz being very noisy, emissivity estimates at 89 GHz could be used for the 150-GHz channel, at least for low zenith angle. We have checked this assumption in the next section by using emissivities at 89 GHz to calculate the Tb at 150 GHz.

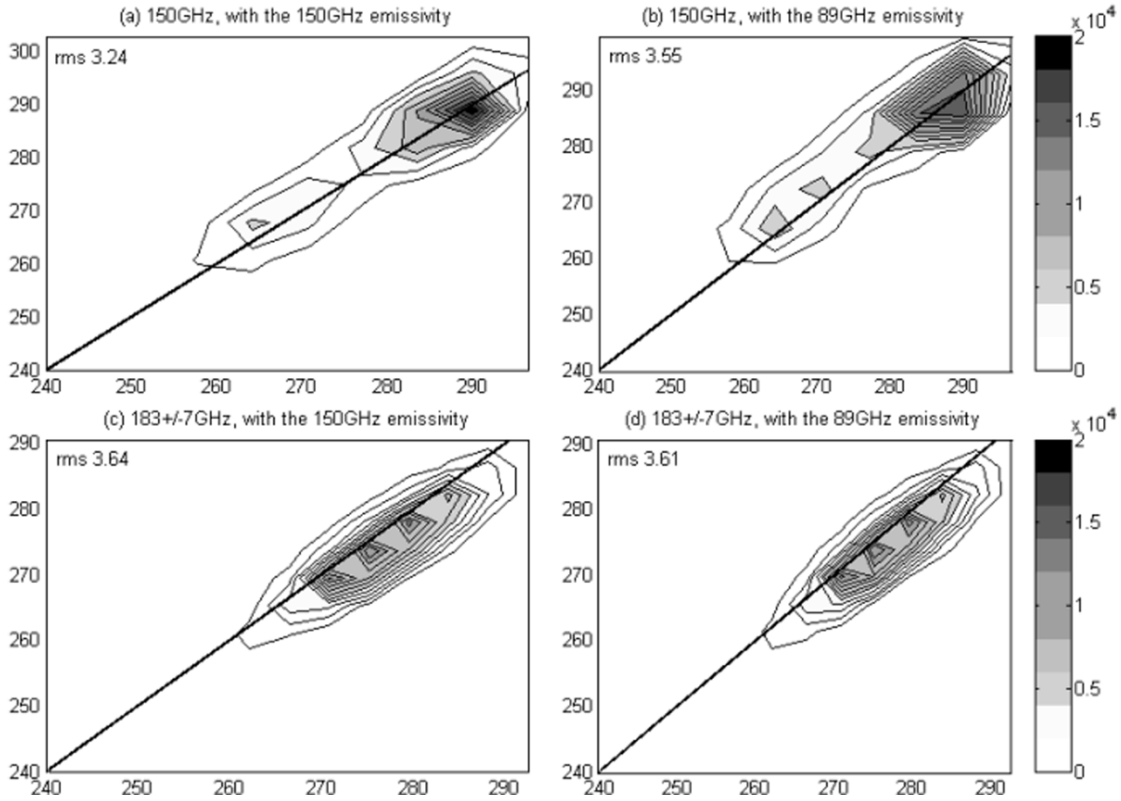

Fig. 9. Density contours of the observed brightness temperature (X axis) versus the simulated brightness temperature (Y axis) over land using odd January 2000 days data for AMSU channels. (a) 150 GHz, using the 150-GHz emissivity calculated using even January days, (b) 150 GHz, using the 89-GHz emissivity calculated using even January days, (c) same as (a) but for 183 $\pm$ 7 GHz, and (d) same as (c) but for 183 $\pm$ 7 GHz. The RMS of errors for (observations-simulations) is added to the plots. The color bar indicates the observations number for each contour class.

IV. Extrapolation of the Calculated Land Surface Emissivities to the Sounding Channels

The emissivity calculations have been performed and analyzed for the AMSU window channels. As already mentioned, similar calculations for sounding channels would not be adequate, due to low atmospheric transmission that translates into limited contribution of the surface radiation at these frequencies. Even the 150-GHz channel calculations have been shown rather noisy as compared to the other window channels, due to lower atmospheric transmission.

Could the emissivities in the sounding channels be accurately estimated from the closest window channels? And therefore, could we use emissivities calculated at window channels to simulate Tbs at the closest sounding channels? Simulating the Tbs in the sounding channels using the averaged emissivities calculated in the closest window channel tests this assumption (Fig. 8). For example, we used the emissivity calculated at 50 GHz to simulate the Tb in the vicinity of the 50-GHz channel (i.e., 52.3- and 53.8-GHz channels) assuming that the emissivity could not change a lot from 50–53 GHz (see the frequency dependence of the emissivity in Section III-D). In the same manner, emissivity at 150 GHz has been used to simulate Tbs at 183.31 $\pm$ 7 and 183.31 $\pm$ 3 GHz.

To evaluate the potential of using surface channels emissivities to simulate Tbs at the closest sounding channels, additional emissivity and Tbs calculations are made. The mean emissivities in the window channels are calculated using the even days in January 2000 for incidence angles lower that 45°. The simulated Tbs are then calculated [using (1)] for window and sounding channels for the odd days of January, using the closest (in frequency) mean emissivities estimated from the even days. That way, the errors derived from the frequency extrapolation will be compared to the natural errors observed for the corresponding frequency. Fig. 8 shows the density contours of the observed Tbs for the odd days in January for nine AMSU frequencies versus the simulated Tbs for the same period using the ATM radiative transfer code, the corresponding ECMWF atmospheric profiles and ISCCP surface temperature, and the mean emissivities calculated in the window channels for the even days for the same month. Good agreements are observed between the measured and the simulated Tbs for all channels, and the agreement is particularly remarkable in the sounding channels. The root mean square (RMS) of errors at window channels is less than 4 (3.44, 3.93, 2.63, 3.80, and, 3.24 at 23.8, 31.4, 50, 89, and 150 GHz). Good results are obtained for the sounding channels: an RMS of $\sim$2 for channels 52 and 53 GHz, and 3.64 for the 183 $\pm$ 7-GHz channel.

The present results show that the emissivity calculation scheme produces quite good estimates of the AMSU Tbs. The radiative transfer model generates a very realistic estimation of the atmospheric contribution since the results for channels less sensitive to surface are also very consistent. For example the RMS of errors at AMSU channels 6, 7, 8, 9, 11, and 12 are 1.41, 1.03, 0.38, 0.45, 1.69, 0.61, and 0.71, respectively.

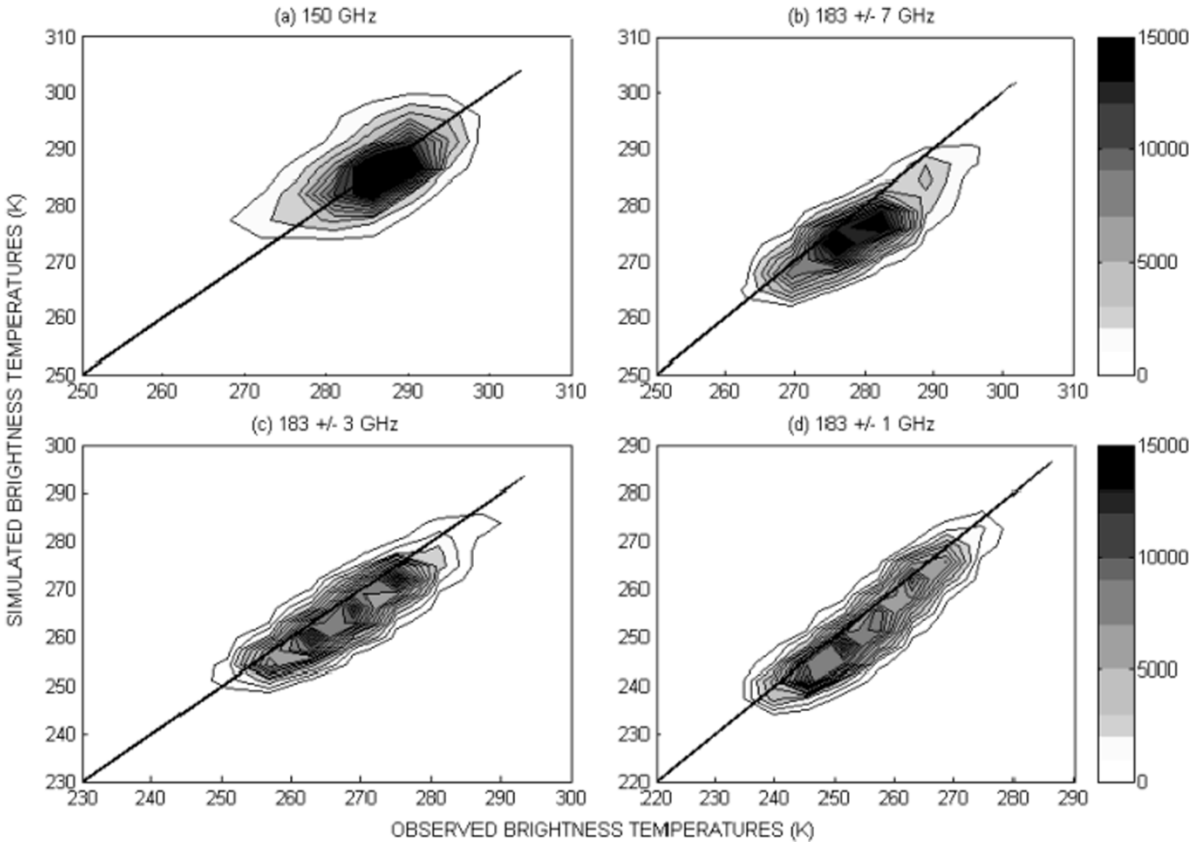

Fig. 10. Density contours of the observed brightness temperature (X axis) versus the simulated brightness temperature (Y axis) over land using 15 days from August 2000 data for AMSU channels. (a) 150 GHz, using the 89-GHz emissivity calculated using July data, (b) same as (a) but for 183 $\pm$ 7 GHz, (c) same as (a) but for 183 $\pm$ 3 GHz, and (d) same as (a) but for 183 $\pm$ 1 GHz.

Given that the 150-GHz emissivity calculations are noisy compared to other surface channels; a further test is performed using the 89-GHz emissivity to simulate the Tb at 150, 183.31 $\pm$ 7, and 183.31 $\pm$ 3 GHz. The corresponding results are given on Fig. 9. The RMS of errors at 150 and 183.31 $\pm$ 7 GHz are then 3.56 and 3.61, respectively.

Emissivity from the 150-GHz channel is noisier in a moist month like July than in January. Fig. 10 compares the simulated Tb for 150, 183.31 $\pm$ 7, 183.31 $\pm$ 3 and, 183.31 $\pm$ 1-GHz channels to the observed Tbs for the 15 first days of August 2000. The simulated Tbs have been calculated using (1) and using the emissivity at 89 GHz estimated with July 2000 data. The agreement between the observed and the simulated Tbs is very good. The use of the emissivity at 89 GHz is a good approximation for the AMSU-B channels (150, 183.31 $\pm$ 7, and 183.31 $\pm$ 3 GHz). This approximation allows us to avoid noise introduced by the 150-GHz retrieved emissivity, which is particularly important in very moist conditions and high zenith angles.

V. Conclusion

The land surface emissivities have been calculated for AMSU window channels for all scanning conditions, for six months in 2000, over Africa, Southern Europe, and the Middle East. The calculation makes use of an up-to-date radiative transfer model (ATM) and is performed for cloud-free AMSU observations. Ancillary data include the ISCCP cloud flags and surface skin temperature, along with the temperature and water vapor profiles from the ECMWF reanalysis. Emissivity maps are presented and show the realistic spatial variations with surface characteristics changes related to vegetation and the presence of open water. The day-to-day variability of the emissivities within a month is lower than 0.02 for all window channels, for low incidence angles (less than 45°). The angular and spectral dependence of the AMSU emissivity is examined for various surfaces. An instrumental AMSU-A problem is evidenced related to an asymmetry in the scan angle behavior. For low incidence angles, the land surface emissivities in the sounding channels (50–60 and 150–183 GHz) could successfully be extrapolated from the calculation in the closest window channels. In a following study, a parameterization of the frequency and angular dependence of the emissivities will be proposed, anchored on accurate emissivity calculations directly derived from satellite observations at 23–150-GHz frequencies and at all incidence angles. The emissivity study is essentially motivated by the need to improve low-level temperature and humidity profiles retrievals over land. The use of the AMSU window emissivities to retrieve atmospheric temperature and humidity information over land using AMSU-A and B measurements has been tested by Karbou *et al.* [14]. The preliminary results are encouraging: the use of reliable land emissivity information helps low- level temperature and humidity profiles retrievals over land (about 2° and 7.5% of temperature and relative humidity RMS errors near the surface, respectively). Further details and investigations about this study will be proposed soon.

The emissivity resulting datasets for AMSU window channels and over Africa, Eurasia, and Eastern South America are available for use by the scientific community. Moreover, additional calculations have been conducted to enlarge the geographic area to the globe.

ACKNOWLEDGMENT

The authors wish to thank F. Chevallier and F. Weng for valuable discussions regarding AMSU calibration. They would like to thank S. Cloche and J. L. Monge for their help to archive and process the ERA40 and AMSU data. They also appreciate comments and suggestions provided by two anonymous reviewers. The ISCCP data have been provided by B.Rossow, AMSU data via the Satellite Active Archive (SAA), and ERA40 temperature-humidity profiles from ECMWF.

REFERENCES

[1] J.-C. Calvet, J.-P. Wigneron, A. Chanzy, S. Raju, and L. Laguerre, "Microwave dielectric proporeties of a silt-loam at high frequencies," *IEEE Trans. Geosci. Remote Sens.*, vol. 33, pp. 634–642, 1995.

[2] B. J. Choudhury, "Reflectivities of selected land surface types at 19 and 37 GHz from SSM/I observations," *Remote Sens. Environ.*, vol. 46, no. 1, pp. 1–17, 1993.

[3] R. E. Dickinson, A. Henderson-Sellers, P. J. Kennedy, and M. F. Wilson, Biosphere-Atmosphere Transfer Scheme (BATS) for the NCAR Community Climate Model, Boulder, CO, 1986.

[4] S. English, "Estimation of temperature and humidity profile information from microwave radiances over different surface types," *J. Appl. Meteorol.*, vol. 38, pp. 1526–1541, 1999.

[5] G. W. Felde and J. D. Pickle, "Retrieval of 91 and 150 GHz earth surface emissivities," *J. Geophys. Res.*, vol. 100, no. D10, pp. 20 855–20 866, Oct 1995.

[6] L. Garand, D. S. Turner, M. Larocque, J. Bates, S. Boukabara, P. Brunel, F. Chevalier, G. Deblonde, R. Engelen, M. Hollingshead, D. Jackson, G. Jedlovec, J. Joiner, T. Kleespies, D. S. McKague, L. McMillin, J.-L. Moncet, J. R. Pardo, P. J. Rayer, E. Salathe, R. Saunders, N. A. Scott, P. Van Delst, and H. Woolf, "Radiance and Jacobian intercomparison of radiative transfer models applied to HIRS and AMSU channels," *J. Geophys. Res.*, vol. 106, pp. 24 017–24 031, 2001.

[7] G. Goodrum, K. B. Kidwell, and W. Winston, *NOAA KLM User's Guide*. Boulder, CO: NOAA, 2000.

[8] N. C. Grody, J. Zhao, R. Ferraro, F. Weng, and R. Boers, "Determination of precipitable water and cloud liquid water over oceans from the NOAA-15 Advanced Microwave Sounding Unit," *J. Geophys. Res.*, vol. 106, pp. 2943–2954, 2001.

[9] T. J. Hewison, "Airborne measurements of forest and agricultural land surface emissivity at millimeter wavelengths," *IEEE Trans. Geosci. Remote Sens.*, vol. 39, no. 2, pp. 393–400, Feb. 2001.

[10] T. J. Hewison and S. English, "Airborne retrieval of snow and ice surface emissivity at millimeter wavelengths," *IEEE Trans. Geosci. Remote Sensing*, vol. 37, no. 4, pp. 1871–1879, Jul. 1999.

[11] T. J. Hewison and R. W. Saunders, "Measurements of the AMSU-B antenna pattern," *IEEE Trans. Geosci. Remote Sensing*, vol. 34, no. 2, pp. 405–412, Mar. 1996.

[12] R. G. Isaacs, Y.-Q. Jin, R. D. Worsham, G. Deblonde, and V. J. Falcone, "The RADTRAN microwave surface emission models," *IEEE Trans. Geosci. Remote Sensing*, vol. 27, no. 2, pp. 433–440, Mar. 1989.

[13] A. S. Jones and T. H. Vonder Haar, "Retrieval of microwave surface emittance over land using coincident microwave and infrared satellite measurements," *J. Geophys. Res.*, vol. 102, no. D12, pp. 13 609–13 626, Jun. 1997.

[14] F. Karbou, F. Aires, C. Prigent, L. Eymard, and J. Pardo, "Atmospheric temperature and humidity profiles over land from AMSU-A and AMSU-B data," presented at the *Microrad04*, Rome, Italy, 2004.

[15] C. Mazler, "Passive microwave signatures of landscapes in winter," *Meteorol. Atmos. Phys.*, vol. 54, pp. 241–260, 1994.

[16] ——, "Seasonal evolution of microwave radiation from an oat field," *Remote Sens. Environ.*, vol. 31, pp. 161–173, 1990.

[17] T. Mo, "AMSU-A antenna pattern corrections," *IEEE Trans. Geosci. Remote Sens.*, vol. 37, no. 1, pp. 103–112, Jan. 1999.

[18] J. C. Morland, D. I. F. Grimes, and T. J. Hewison, "Satellite observations of the microwave emissivity of a semi-arid land surface," *Remote Sens. Environ.*, vol. 77, no. 2, pp. 149–164, 2001.

[19] J. C. Morland, D. I. F. Grimes, G. Dugdale, and T. J. Hewison, "The estimation of land surface emissivities at 24 GHz to 157 GHz using remotely sensed aircraft data," *Remote Sens. Environ.*, vol. 73, no. 3, pp. 323–336, 2000.

[20] J. R. Pardo, J. Cernicharo, and E. Serabyn, "Atmospheric Transmission at Microwave (ATM): An improved model for millimeter/submillimeter applications," *IEEE Trans. Antennas Propagat.*, vol. 49, no. 12, pp. 1683–1694, Dec. 2001.

[21] C. Prigent, J. -Munier, G. Ruffié, and J. Roger, "Interpretation of passive microwave satellite observations over Oman and Egypt," presented at the *EGS-AGU*, Nice, France, 2003.

[22] C. Prigent, J. P. Wigneron, B. Rossow, and J. R. Pardo, "Frequency and angular variations of land surface microwave emissivities: Can we estimate SSM/T and AMSU emissivities from SSM/I emissivities?," *IEEE Trans. Geosci. Remote Sens.*, vol. 38, no. 5, pp. 2373–2386, Sep. 2000.

[23] C. Prigent, W. B. Rossow, and E. Matthews, "Global maps of microwave land surface emissivities: Potential for land surface characterization," *Radio Sci.*, vol. 33, pp. 745–751, 1998.

[24] ——, "Microwave land surface emissivities estimated from SSM/I observations," *J. Geophys. Res.*, vol. 102, pp. 21 867–21 890, 1997.

[25] W. B. Rossow and L. C. Garder, "Cloud detection using satellite measuremenst of infrared and visible radiances for ISCCP," *J. Clim.*, vol. 6, pp. 2341–2369, 1993a.

[26] ——, "Validation of ISCCP cloud detection," *J. Clim.*, vol. 6, pp. 2370–2393, 1993b.

[27] W. B. Rossow and R. A. Schiffer, "ISCCP cloud data products," *Bull. Amer. Meteorol. Soc.*, vol. 72, pp. 2–20, 1991.

[28] F. Weng, L. Zhao, R. Ferraro, G. Poe, X. Li, and N. Grody, "Advanced Microwave Sounding Unit cloud and precipitation algorithms," *Radio Sci.*, vol. 38, pp. 8,086–8,096, 2003.

[29] F. Weng, B. Yan, and N. Grody, "A microwave land emissivity model," *J. Geophys. Res.*, vol. 106, no. D17, pp. 20 115–20 123, 2001.

[30] J.-P. Wigneron, D. Guyon, J.-C. Calvet, G. Courrier, and N. Bruiguier, "Monitoring coniferous forest characteristics using a multifrequency microwave radiometry," *Remote Sens. Environ.*, vol. 60, pp. 299–310, 1997.

[31] L. Zhao and F. Weng, "Retreival of ice cloud parameters using the Advanced Microwave Sounding Unit (AMSU)," *J. Appl. Meteorol.*, vol. 41, pp. 384–395, 2002.

Fatima Karbou received the engineering degree in topography from the Institut Agronomique et Vétérinaire Hassan II, Rabat, Morocco, in 1999, and the Ph.D. degree in physics of remote sensing from Versailles Saint Quentin en Yvelines University, Vélizy, France, in 2004.

In September 2000 and during one year, she joined the ACRI research firm team at Sophia-Antipolis, France, as a Research Engineer. She worked on an air pollution simulator in both urban and rural environments and on NOAA instruments level 1 and 2 data processing tools. Her main fields of interest include the use of passive microwave instruments to estimate and analyze the land emissivities and to retrieve atmospheric parameters over land.

Catherine Prigent received the Ph.D degree in physics from Paris University, Paris, France, in 1988.

Since 1990, she has been a Researcher for the Centre National de la Recherche Scientifique (CNRS) in the Paris Observatory. From 1995 to 2000, she was on leave from the CNRS and worked at the NASA Goddard Institute for Space Studies, Columbia University, New York. She is now back at Paris Observatory. Her research interests focus on passive microwave remote sensing of the earth. She first worked on modeling of the sea surface emissivities at microwave wavelengths and on the estimation of atmospheric parameters over ocean from microwave measurements. At present, her main interests include calculation and analysis of microwave land surface emissivities and estimation of atmospheric and surface parameters over land from microwave observations using variational and neural network methods. She is also involved in satellite remote sensing of clouds with the analysis of passive microwave observations over convective cloud structures.

Laurence Eymard graduated from Ecole Normale Superieure and Université Pierre et Marie Curie, Paris, France, in 1978. She received the Ph.D. degree in physics of the atmosphere in 1985.

She is currently a Senior Scientist (Directeur de Recherche) at the Centre National de la Recherche Scientifique (CNRS), Head of Laboratoire d'Ocanographie et du Climat Expérimentations et Approches Numériques (CNRS/IPSL/LOCEAN), Université Pierre et Marie Curie, Paris. Her Main research domains are atmosphere dynamics (boundary layer) and hydrological cycle, ocean—atmosphere interactions, and microwave radiometry. She coordinated experimental studies of the ocean–atmosphere interactions (SEMAPHORE, CATCH/FASTEX). She is principal investigator (PI) of the ERS/ENVISAT and Jason altimeter missions, and she is in charge of the in-flight calibration/validation of ERS microwave radiometers. She is also the PI of a new humidity sounder (SAPHIR) on the Megha/Tropique Indian French mission project to be launched in 2009.

Juan R. Pardo received the degree in physics from Complutense University of Madrid, Madrid, Spain, in 1991, and the Ph.D. degree in astrophysics and spatial technology from Pierre et Marie Curie University, Paris, France, in 1996.

Since then, he has been a Postdoctoral Research Fellow supported by the U.S. National Science Foundation at the NASA Goddard Institute for Space Studies, Columbia, New York, and at the California Institute of Technology, Pasadena. In 2001, he joined the Consejo Superior de Investigaciones Científicas, Madrid, as a Research Associate. His main research interests are microwave and IR spectroscopy, observational techniques in submillimeter astronomy, interstellar and circumstellar media, radiative transfer in planetary atmospheres, and terrestrial and planetary remote sensing from ground and satellite platforms. He has made several contributions to these areas in the past, including the ATM model used in this work.